



SPE 149690-PA

Accurate Modelling of Faults by Multipoint, Mimetic, and Mixed Methods

Halvor M. Nilsen, K.-A. Lie, SPE, and Jostein R. Natvig, SINTEF ICT.

Copyright 2010, Society of Petroleum Engineers

This paper was prepared for peer review in the SPE Journal.

Contents of the paper have not been reviewed by the Society of Petroleum Engineers and are subject to correction by the author(s). The material does not necessarily reflect any position of the Society of Petroleum Engineers, its officers, or members. Electronic reproduction, distribution, or storage of any part of this paper without the written consent of the Society of Petroleum Engineers is prohibited. Permission to reproduce in print is restricted to an abstract of not more than 300 words; illustrations may not be copied. The abstract must contain conspicuous acknowledgment of SPE copyright.

Abstract

The predominant way of modeling faults in (industry-standard) flow simulators is to introduce so-called transmissibility multipliers in the underlying two-point discretization. Although this approach provides adequate accuracy in many practical cases, two-point discretizations are only consistent for K-orthogonal grids and may introduce significant discretization errors for grids that severely depart from being K-orthogonal. Such grid-distortion errors can be avoided by lateral or vertical stair-stepping of deviated faults, at the expense of errors in the geometrical fault description. In other words, modelers have the choice of either making (geometrical) errors by adapting faults to a grid that is almost K-orthogonal or introducing discretization errors because of the lack of K-orthogonality if the grid is adapted to deviated faults.

We propose a method for accurate description of faults in solvers based on a hybridized mixed or mimetic discretization, which also includes the MPFA-O method. The key idea is to represent faults as internal boundaries and calculate fault transmissibilities directly instead of using multipliers to modify grid-dependent transmissibilities. The resulting method is geology-driven and consistent for cells with planar surfaces and thereby avoids the grid errors inherent in the two-point method. We also propose a method to translate fault transmissibility multipliers into fault transmissibilities. This makes our method readily applicable to reservoir models that contain fault multipliers.

Introduction

Faults can either act as conduits for fluid flow in subsurface reservoirs or create flow barriers and introduce compartmentalization that severely affects fluid distribution and/or reduces recovery. To make flow simulations reliable and predictive, it is crucial to understand and accurately account for the impact that faults have on fluid flow. On a reservoir scale, faults are generally volumetric objects that can be described in terms of displacement and petrophysical alteration of the surrounding host rock. However, lack of geological resolution in simulation models means that fault zones are commonly modeled as surfaces that explicitly approximate the faults' geometrical properties.

Modeling faults can be divided into two subtasks: geometrical representation and modeling of hydraulic properties. This modeling has traditionally been dictated by two key technologies within subsurface modeling: stratigraphic grids (corner-point, PEBI, etc) and discretization schemes based on two-point flux approximations (TPFA). Stratigraphic grids are built by extruding 2D tessellations of geological horizons in the vertical direction or in a direction following major fault surfaces to form volumetric cells. Such a gridding strategy usually requires significant simplifications in the fault description. In the subsequent gridding process, one is faced with two choices: The extrusion direction and the cell faces in the grid can be set to follow major fault surfaces, which gives grid cells that are not K-orthogonal and hence susceptible to large discretization errors when used together with a traditional two-point method, see (Aavatsmark, 2007; Wu and Parashkevov, 2009). These discretization errors can be reduced by using a more accurate discretization. In recent years, there has been significant research into multipoint flux-approximation (MPFA) schemes (Aavatsmark et al., 2001), mixed finite elements (Brezzi and Fortin, 1991), or mimetic methods (Brezzi et al., 2005) that all are consistent and convergent. Alternatively, one can choose a vertical extrusion direction and replace deviated fault surfaces by stair-stepped approximations so that the faults zig-zag in directions not aligned with the grid. This will create cells that are mostly K-orthogonal and hence limit the two-point discretization errors. Likewise, areal distortions can be reduced by using 2.5D Voronoi grids (Wu and Parashkevov, 2009; Branets et al., 2009). Another alternative is to use unstructured grids to adapt to complex fault networks (Gringarten et al., 2008). This requires the development of flexible and robust discretizations that are capable of handling (irregular) polyhedral cells. The purpose of the paper is to develop a method that can incorporate subgrid descriptions of faults into multipoint, mixed, and mimetic discretization schemes and hence make these methods more applicable to modeling of faulted reservoirs; we do *not* aspire to give a thorough discussion of how multipoint discretization or advanced gridding methods can be used to reduce grid-orientation errors for faulted reservoirs.

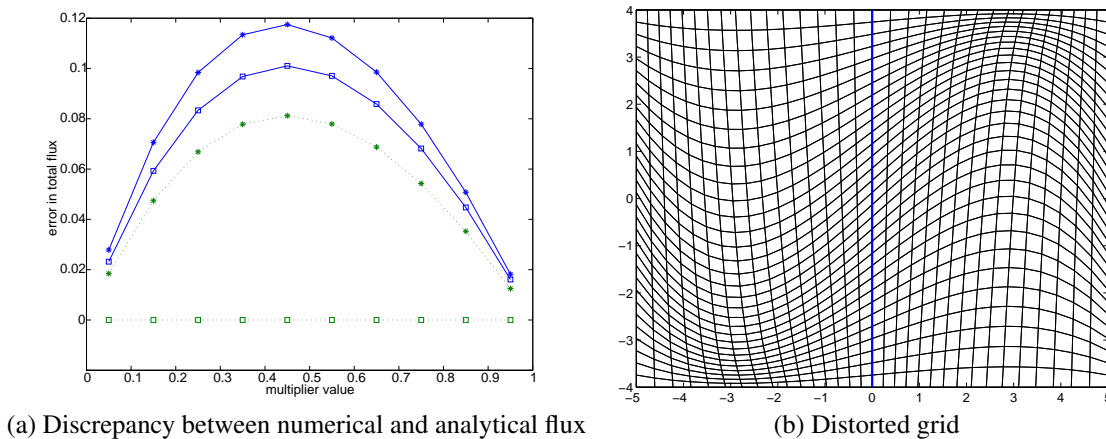


Fig. 1—Flow from left to right over a fault in a 2D domain. (a) The discrepancy between the analytical flux solution and the flux computed by applying the TPFA multiplier directly in two consistent schemes (solid lines=mimetic, dotted lines=MPFA-O) as a function of multiplier values; Square markers denote a 32×32 orthogonal grid while star markers denote the distorted 32×32 grid. (b) The distorted grid.

The flow between two adjacent cells in a standard flow simulator is determined by the transmissibility that represents the volume-weighted average permeability. Faults affect the transmissibilities geometrically by introducing new cell-to-cell connections and by changing the contact areas between two cells that are juxtaposed over a fault surface. Similarly, the effective transmissibility is changed by fault-zone material interposed between cross-fault juxtaposed cells. To capture these effects, it is common to introduce transmissibility multipliers that account for the reduced or increased permeability for each cross-fault connection. Fault multipliers are typically calculated as empirical functions of the fault displacement, the fault thickness (as a function of displacement), and the clay fraction of the sequence that has moved past each point on the fault, see e.g., Yielding et al. (1997); Manzocchi et al. (1999); Sperrevik et al. (2002). These multipliers are highly grid dependent and strictly associated with a connection between two grid cells rather than with the fault itself. Hence, if one wants to refine the grid, fault permeabilities must generally be recalculated and then translated back to new multiplier values.

Fault multipliers are not a good solution from a modeling point of view because any given multiplier value will be tied to a particular discretization and introducing these values into another (consistent) scheme will produce large pointwise errors. We will illustrate this by an example.

Example: 2D flow channel. Consider the domain $(x, y) \in [-5, 5] \times [-4, 4]$ with homogeneous, isotropic permeability and a vertical fault at $x = 0$, modeled using prescribed multiplier values corresponding to a TPFA scheme. A straightforward way of introducing the multiplier for the mixed or mimetic method is to divide the diagonal of the mass matrix with the multiplier value. Similarly, for the MPFA-O method we multiply the row of the transmissibility matrix associated with a particular grid face with the corresponding multiplier. The mimetic and MPFA-O methods will be described in detail on page 4.) To assess the accuracy of the resulting schemes, we consider two different grids, an orthogonal grid and a distorted grid, and use the following computational setup: no-flow boundary conditions along the upper and lower boundaries and a pressure drop in the x -direction to produce an analytical solution with unit flux density at the outflow boundary. Figure 1 shows the corresponding errors, as a function of multiplier values, measured as the discrepancy in L^2 -norm from the analytical overall flux. We see that the straightforward implementation of multipliers for these two methods introduces errors for non-orthogonal grids. For the mimetic method, there is also an error for the orthogonal grid that can be characterized exactly. For two cells separated by a face with multiplier m , the relative flux error in a pressure-driven case is

$$E(m) \propto \frac{m(1-m)(1-\frac{1}{C})}{(1-m)\frac{1}{C} + m}, \quad (1)$$

where C is the ratio between the TPFA transmissibility and the inverse of the diagonal of the mass matrix of the mimetic (or mixed-hybrid) method; a derivation is given in the appendix. A similar expression will be valid for any simple method to incorporate multipliers that associates the flow in the direction of the fault only with the faulted face, because the key to a consistent method is to use pressure values at points not only associated with the cell and the faulted face.

Motivated by the above example, we propose that faults are modeled as internal boundaries in the reservoir domain so that they are given a geological meaningful form and represented as separate entities that can be assigned physical properties like width and permeability. Flow through each fault can then be incorporated using physical principles (Darcy's law and flux continuity) and not through a grid-dependent manipulation of (two-point) transmissibilities.

Treating faults as internal boundaries is related to ideas used to model flow in fracture network, see (Hoteit and Firoozabadi, 2008; Martin et al., 2005) and references therein. In a majority of these papers, one is primarily interested in the flow *along* the lower-dimensional object and assumes no pressure drop across it. Herein, we consider the opposite case, assuming no flow along, but a (significant) pressure-drop across, the lower-dimensional object (fault).

To discretize the flow equations with internal boundaries, we propose two simple algorithms, one suited for methods formulated on a mixed form and one for methods formulated on hybridized mixed form. The basic unknowns in a hybrid formulation are the face pressures. If we allow these face pressures to take one-sided values at the internal boundaries, flow through faults can easily be incorporated by specifying fault transmissibilities that can be calculated directly from transmissibility multipliers. The method for mixed discretizations is similar, but needs to single out closed faults as a geometrical property. We also propose a simple formula to calculate fault transmissibilities from a given set of multipliers, following Manzocchi et al. (1999).

Flow Equations and Hybrid Discretization

To keep technical details at a minimum, we will in the following consider a simplified set of single-phase flow equations,

$$\nabla \cdot \vec{v} = q, \quad \vec{v} = -\frac{\mathbf{K}}{\mu} \nabla p, \quad \text{in } \Omega. \quad (2)$$

Here \vec{v} denotes the Darcy velocity, p pressure, \mathbf{K} permeability, and μ viscosity. All external boundaries $\partial\Omega$ are equipped with either prescribed pressure (Dirichlet) or prescribed flux (Neumann) boundary conditions.

Reservoir geometries and petrophysical properties are represented by volumetric grids that typically adapt to geological horizons and major faults. This requires grids that are flexible with respect to geometry (and topology). Stratigraphic grids have been popular for many years and are the current industry standard. These grids are formed by extruding areal grids defined along geological surfaces to form volumetric descriptions; the most common formats are hexahedral corner-point grids or 2.5D Voronoi grids. This results in grids that are typically mismatched and contain non-neighboring cell topologies across fault faces. Recently, more complex methods based on unstructured grids are gaining in popularity as a means to modeling complex fault systems, horizontal and multilateral wells, etc. (Gringarten et al., 2008; Branets et al., 2009). In either case, geometrically realistic models of faulted reservoirs will generally contain polyhedral cells and/or complex grid-cell connectivities. Herein, we assume all grids to be matching. This means that non-matching, stratigraphic grids have been preprocessed to form a set of non-overlapping, polyhedral cells. While straightforward for planar faces, this may constitute a major challenge for curved (fault) faces, which may give models that have interior gaps or overlapping cells. Consistent treatment of such grid mismatches is beyond this paper; herein, we simply assume that one is able to subdivide mismatched curved surfaces into a unique set of planar surface patches.

As stated in the introduction, we propose to model all interior faults as internal boundaries, over which we prescribe a set of jump conditions,

$$(\vec{v} \cdot \vec{n})^+ = (\vec{v} \cdot \vec{n})^-, \quad \vec{v} \cdot \vec{n} = t_f(p^+ - p^-), \quad \text{at } \Gamma, \quad (3)$$

where Γ denotes the fault surface, \vec{n} is the surface normal, and the superscripts \pm denote the one-sided values on opposite sides of the surface. The new feature of our fault modeling is the scalar fault transmissibility density t_f defined as the transmissibility per unit area on Γ , which we will come back to later. Together, Eq. 2 and Eq. 3 give a Laplace equation with coupled boundaries, which will be our starting point for deriving a consistent and convergent set of discrete flow equations for grids with planar faces.

In summary, we start by dividing the computational domain Ω into a set $\{\Omega_i\}$ of N non-overlapping polyhedral cells, where each cell i can have a varying number of n_i planar faces that match the faces of the cell's neighbors. Now, let \mathbf{u}_i be the vector of outward fluxes over the faces of Ω_i and let p_i denote the pressure at the cell center and $\boldsymbol{\pi}_i$ the face pressures. Discretization methods used for reservoir simulation are constructed to be locally conservative and exact for linear solutions. Such schemes can be written in a form that uses Darcy's law to relate the three quantities \mathbf{u} , p , and $\boldsymbol{\pi}$ through a matrix \mathbf{T}_i of one-sided transmissibilities,

$$\mathbf{u}_i = \mathbf{T}_i(\mathbf{e}_i p_i - \boldsymbol{\pi}_i), \quad \mathbf{e}_i = (1, \dots, 1)^\top. \quad (4)$$

The one-sided transmissibilities are associated with the pressure difference between cell centers and pressure-continuity points on cell faces. Together with continuity of fluxes and face pressures, Eq. 4 can be used to derive the corresponding, standard transmissibilities that are used to express Darcy's law in terms of pressure differences between cell centers.

Augmenting Eq. 4 with flux and pressure continuity across cell faces, we get the following linear system

$$\begin{bmatrix} \mathbf{B} & \mathbf{C} & \mathbf{D} \\ \mathbf{C}^\top & \mathbf{0} & \mathbf{0} \\ \mathbf{D}^\top & \mathbf{0} & \mathbf{0} \end{bmatrix} \begin{bmatrix} \mathbf{u} \\ -p \\ \boldsymbol{\pi} \end{bmatrix} = \begin{bmatrix} \mathbf{0} \\ \mathbf{q} \\ \mathbf{0} \end{bmatrix}, \quad (5)$$

where the first row in the block-matrix equation corresponds to Eq. 4 for all grid cells. Thus, \mathbf{u} denotes the outward face fluxes ordered cellwise (fluxes over interior faces and faults appear twice with opposite signs), p denotes the cell pressures, and $\boldsymbol{\pi}$ the face pressures, where each side of a fault is considered as separate faces. The matrices \mathbf{B} and \mathbf{C} are block diagonal with each block corresponding to a cell. For the two matrices, the i 'th blocks are given as \mathbf{T}_i^{-1} and \mathbf{e}_i , respectively. Similarly, each column of \mathbf{D} corresponds to a unique face and has one (for boundary faces) or two (for interior faces) unit entries corresponding to the index(s)

of the face in the cellwise ordering. Eq. 5 is solved by a formal, standard Gauss elimination of the block system. This gives a *symmetric positive-definite* system (the Schur complement) for the face pressures,

$$(D^T B^{-1} D - F^T L^{-1} F) \pi = F^T L^{-1} q, \quad F = C^T B^{-1} D, \quad L = C^T B^{-1} C.$$

Given the face pressures, the cell pressures and fluxes can be reconstructed by back-substitution, i.e., solving

$$Lp = q + F^T \pi, \quad Bv = Cp - D\pi.$$

Here, the matrix L is by construction diagonal and computing fluxes is therefore an inexpensive operation.

Specific Discretization Schemes

Examples of schemes that can be written as in Eq. 4 include the two-point flux-approximation method (Aziz and Settari, 1979), the lowest-order mixed finite-element methods (Brezzi and Fortin, 1991), multipoint flux approximation schemes (Aavatsmark et al., 1994; Edwards and Rogers, 1994; Aavatsmark, 2002), and recent mimetic finite-difference methods (Brezzi et al., 2005). Two-point discretizations give diagonal T_i and are not convergent for general grids. Mixed, multipoint, and mimetic methods lead to full matrices T_i . To ease the presentation, we only consider schemes that may be written in hybridized mixed form and assume that the schemes have a single pressure-continuity point on each interface. Note that these restrictions, which exclude some multipoint schemes, are only necessary to give a uniform formulation of the schemes below. The underlying principles of the methodology, however, may be applied to any reasonable scheme.

We will in the following consider three specific schemes: the standard two-point flux-approximation (TPFA) scheme, a mimetic finite-difference (MFD) scheme, and a multipoint flux-approximation (MPFA-O) scheme.

TPFA: The two-point scheme approximates the flux across a cell face in terms of the difference in pressure between the centers of the adjacent cells. Using the notation of one-sided transmissibilities from Eq. 4, the simplest form¹ of the TPFA scheme reads

$$T_{i,k} = \bar{c}_{ik} \cdot \mathbf{K} \bar{n}_k A_k / |\bar{c}_{ik}|^2, \quad (6)$$

where A_k is the face area, \bar{n}_k is the normal of the face, and \bar{c}_{ik} is the vector from the centroid of cell i to the centroid of the k th face, see Figure 2. Although monotone and robust, the scheme is only consistent and convergent if each grid cell satisfies the K-orthogonality conditions that $\mathbf{K} \bar{n}_k$ is parallel to \bar{c}_k , where \bar{n}_k is normal vector of face k and \bar{c}_k is the difference between the face centroid and cell centroid. If the TPFA method is used to discretize Eq. 2 on grids that are not K-orthogonal, the scheme will produce different results depending on the orientation of the grid (grid-orientation effects) and will generally converge to a wrong solution. Despite this shortcoming, the TPFA discretization is the industry standard for practical reservoir simulation.

MPFA-O: Multipoint flux-approximation schemes aim to amend the shortcomings of the TPFA scheme. Herein, we only give a quick recap of the basic idea; the interested reader is referred to Aavatsmark (2002), for instance, for more details. Consider an orthogonal grid and assume that \mathbf{K} is a constant tensor with nonzero off-diagonal terms. Let Γ_{ij} denote the interface between two adjacent cells in the x -coordinate direction and let \bar{n}_{ij} denote the normal to Γ_{ij} . The flux in the x -direction is then given as,

$$\int_{\Gamma_{ij}} \bar{v} \cdot \bar{n}_{ij} ds = - \int_{\Gamma_{ij}} \mu^{-1} \left(K_{xx} \partial_x p + K_{xy} \partial_y p + K_{xz} \partial_z p \right) ds.$$

This expression involves derivatives in three orthogonal directions. To obtain consistent interfacial fluxes for grids that are not K-orthogonal, one needs to know the partial derivatives parallel to the cell faces, which obviously cannot be estimated based on the cell values p_i and p_j . More than two cell values are therefore needed, hence giving a full transmissibility matrix in Eq. 4.

As an example of multipoint methods, we consider the MPFA-O method. We start by defining an interaction region around each corner-point in the grid, restricted by faces that connect cell centroids and face centroids. For each interaction region, we define a set of linear (pressure) functions that are required to be continuous at the centroids of the cell faces and flux-continuous across the face patches that lie inside the interaction regions. To obtain a globally coupled system, the continuity requirements are used to express the gradients of the linear functions, and hence the corresponding flux across the face patches of the interaction region, in terms of the unknown cell pressures p_i . This requires the solution of a local system of equations. Finally, the cell pressures are determined by summing the fluxes across all face patches and requiring mass conservation. Transmissibilities are assembled as part of this process. Rather than using the original MPFA-O formulation, we will herein utilize the equivalent local-flux mimetic formulation (Klausen and Stephansen, 2008; Lipnikov et al., 2009).

¹As written, this does not always yield a positive value for the two-point transmissibility. To ensure positive transmissibilities in the model examples, we define the face centroids as the arithmetic middle of the associated corner-point nodes and the cell centroids as the arithmetic middle of the top and bottom surface centroids. We believe that this is the modification used in a leading commercial simulator.

Mimetic: There are two ways to view a mimetic method. First, one can see it as a finite-difference counterpart of a mixed finite-element method, in which the velocity approximation space is replaced by a space of fluxes defined over the cell faces, giving a variational formulation with *discrete* inner product. Alternatively, a mimetic method may be seen as a multipoint finite-volume method that exactly mimics certain properties of the underlying continuous problem. Herein, we consider a mimetic method that reproduces linear flow exactly on arbitrary polyhedral cells. To this end, we require that the method is exact for any linear pressure field $p = \vec{x} \cdot \vec{a} + c$. Combined with Darcy's law, this gives two equations

$$u_k = -A_k \vec{n}_k \cdot \mathbf{K} \vec{a}, \quad p_i - \pi_k = \vec{c}_{ik} \cdot \vec{a},$$

where u_k denotes the flux over face k and the remaining quantities are defined in Figure 2. From Eq. 4, we see that the one-sided transmissibilities \mathbf{T} must satisfy the matrix equation

$$\mathbf{T} \tilde{\mathbf{C}} = \mathbf{N} \mathbf{K},$$

where $\tilde{\mathbf{C}}$ denotes the matrix of centroid differences \vec{c}_{ik} and each row in \mathbf{N} corresponds to a given face k and contains the outer normal \vec{n}_k of the cell at this face scaled with the face area. A family of valid solutions is

$$\mathbf{T} = \frac{1}{|\Omega_i|} \mathbf{N} \mathbf{K} \mathbf{N}^\top + \tilde{\mathbf{T}}, \quad (7)$$

where $|\Omega_i|$ denotes the cell volume and $\tilde{\mathbf{T}}$ spans the null space of $\tilde{\mathbf{C}}$, i.e., $\tilde{\mathbf{T}} \times \tilde{\mathbf{C}} = 0$. There are many ways to choose the matrix $\tilde{\mathbf{T}}$; the number of degrees of freedom is $p(p+1)/2$, where p equals the number of cell faces minus the number of space dimensions. This can be utilized to specify schemes that reduce to methods like TPFA or the standard mixed Raviart–Thomas method on Cartesian grids. Herein, we have made the following choice (Aarnes et al., 2008)

$$\mathbf{T} = \frac{1}{|\Omega_i|} \mathbf{N} \mathbf{K} \mathbf{N}^\top + \frac{6}{d|\Omega_i|} \text{tr}(\mathbf{K}) \mathbf{A} (\mathbf{I} - \mathbf{Q} \mathbf{Q}^\top) \mathbf{A}, \quad (8)$$

where d is the number of space dimensions, \mathbf{A} is the diagonal matrix of face areas A_k and the trace $\text{tr}(\mathbf{K})$ denotes the sum of the elements on the diagonal of the permeability tensor \mathbf{K} . For consistency, the second term in the mimetic transmissibility matrix should be in the null space of $\tilde{\mathbf{C}}$. To achieve this, the matrix \mathbf{Q} is a basis for the column space of $\mathbf{A} \tilde{\mathbf{C}}$ (constructed using a standard orthogonalization technique from linear algebra) which makes the matrix $\mathbf{I} - \mathbf{Q} \mathbf{Q}^\top$ a projection onto the null space of $\mathbf{A} \tilde{\mathbf{C}}$.

The mimetic method is particularly simple to implement for fully unstructured polyhedral grids and is normally our method-of-choice if a two-point scheme is not sufficiently accurate on a fully unstructured and geometrically complex grid.

Discretization Across Faults

In the following, we will show that the correct way to treat transmissibilities T_f (or more correctly, transmissibility densities) associated with internal boundaries such as faults or shale layers is to replace Eq. 4 by

$$\mathbf{u}_i = \left(\mathbf{T}_i^{-1} + \mathbf{F} \right)^{-1} (\mathbf{e}_i p_i - \boldsymbol{\pi}_i), \quad \mathbf{e}_i = (1, \dots, 1)^\top, \quad (9)$$

where \mathbf{F} is diagonal with $F_{kk} = \frac{1}{2} T_{f,k}^{-1}$ if there is a transmissibility $T_{f,k}$ associated with face k (zero otherwise). It is apparent from this equation that it is impossible to introduce the effect of fault transmissibilities $T_{f,k}$ through a multiplicative factor such as a fault multiplier. To show this, we first introduce the jump conditions Eq. 3 at the internal boundaries as extra equations in Eq. 5. The jump conditions are discretized as follows,

$$u_f^+ = T_f (\pi_f^- - \pi_f^+), \quad u_f^- = T_f (\pi_f^+ - \pi_f^-), \quad (10)$$

where the fault transmissibility is defined as (see Figure 2)

$$T_f = A K_f / d_f = A k_f. \quad (11)$$

To incorporate the jump conditions into Eq. 5, we extend $\boldsymbol{\pi}$ by the one-sided face pressures π^\pm along Γ and split² each column of \mathbf{D} that corresponds to a face on Γ into two columns, each having a single nonzero entry. This gives a slightly enlarged matrix $\tilde{\mathbf{D}}$ and vector $\tilde{\boldsymbol{\pi}}$. Moreover, we introduce a symmetric block-diagonal matrix \mathbf{E} containing a 2×2 -block of fault transmissibilities for each internal boundary condition, Eq. 10. Then, the extended mixed hybrid system reads

$$\begin{bmatrix} \mathbf{B} & \mathbf{C} & \tilde{\mathbf{D}} \\ \mathbf{C}^\top & \mathbf{0} & \mathbf{0} \\ \tilde{\mathbf{D}}^\top & \mathbf{0} & \mathbf{E} \end{bmatrix} \begin{bmatrix} \mathbf{u} \\ -p \\ \tilde{\boldsymbol{\pi}} \end{bmatrix} = \begin{bmatrix} \mathbf{0} \\ \mathbf{q} \\ \mathbf{0} \end{bmatrix}. \quad (12)$$

²Each column of \mathbf{D} corresponds to a unique face and has two unit entries (for all interior faces) corresponding to the indices of the face in the cellwise ordering. This reflects that each unknown in $\boldsymbol{\pi}$ appears in two one-sided discretizations, one for each cell that share the face. In the expanded system, each column of $\tilde{\mathbf{D}}$ has a single nonzero entry corresponding to the index of π^+ or π^- , respectively, that both appear in a single one-sided discretization.

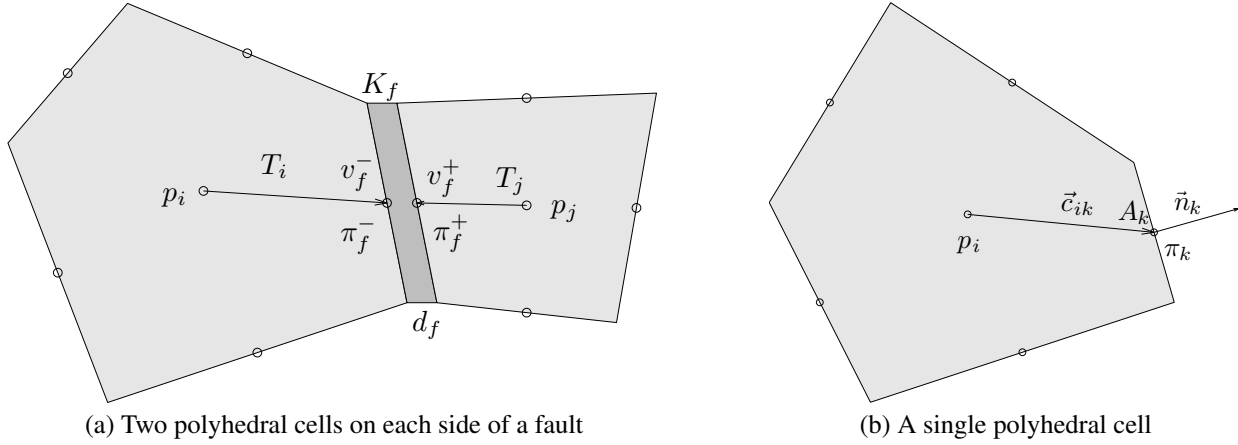


Fig. 2—(a) Two cells on each side of a fault zone (dark gray) with permeability K_f and width d_f ; the width of the fault zone is highly exaggerated to show the entities used to derive the corresponding fault transmissibility multipliers. (b) The quantities used to define one-sided transmissibilities in a single polyhedral cell.

The system can be solved using the standard Schur complement approach outlined above. Alternatively, we can introduce a unique fault pressure $\pi = (\pi_f^+ + \pi_f^-)/2$ that can be used to eliminate the one-sided pressures from Eq. 12. Inserting $\pi_f^\pm = 2\pi - \pi^\mp$ into Eq. 10, we obtain

$$\pi_f^+ = \frac{u_f^+}{2T_f} + \pi, \quad \pi_f^- = \frac{u_f^-}{2T_f} + \pi. \quad (13)$$

Then, writing Eq. 13 as $\tilde{D}\tilde{\pi} = D\pi + Fu$, where F is a diagonal matrix of inverse fault transmissibilities (divided by two), imposing flux continuity across the faults explicitly, we get the following system

$$\begin{bmatrix} \tilde{B} & C & D \\ C^T & 0 & 0 \\ D^T & 0 & 0 \end{bmatrix} \begin{bmatrix} u \\ -p \\ \pi \end{bmatrix} = \begin{bmatrix} 0 \\ q \\ 0 \end{bmatrix}, \quad (14)$$

where $\tilde{B} = B + F^{-1}$. Note that if Eq. 14 is a two-point flux discretization, then B^{-1} is a diagonal matrix of one-sided transmissibilities, and \tilde{B}^{-1} is the harmonic average of one-sided transmissibilities and fault transmissibilities. Hence, we see that the correct way to treat fault transmissibilities T_f is to replace Eq. 4 by Eq. 9. (An open-source implementation is available in the open-source Matlab Reservoir Simulation Toolbox (MRST, 2011; Lie et al., 2011)). The method can easily be extended to discretization schemes that are formulated using multiple pressure-continuity points by simply using the same expansion of the π -vector for each continuity point.

In the discussion above, we have assumed a simple single-phase flow model. However, the formulas presented above apply (almost) verbatim to incompressible multiphase flow models. Likewise, the method can be extended to compressible flow if the corresponding nonlinear flow equations can be linearized and discretized in a form analogous to Eq. 5, e.g., as presented by Krogstad et al. (2009) for compressible three-phase black-oil models.

Fault Multipliers and Fault Transmissibilities

In the previous section, we assumed that the fault transmissibility could be computed from knowledge of the fault permeability K_f and the fault width d_f , or from the fault transmissibility density t_f . Unfortunately, these quantities are not available in most industry-standard simulation models given, e.g., on the corner-point grid format. In this section, we will therefore show how fault transmissibilities can be constructed from a set of prescribed two-point multipliers, which are the predominant way of representing the hydraulic properties of faults.

We will follow Manzocchi et al. (1999), who formulated a method for calculating fault transmissibilities from known fault permeabilities with the help of the underlying physical properties of the faults. We consider a pair of polyhedral cells with a semi-permeable fault between them, as illustrated in Figure 2. We assume that the fault thickness is so small that it does not affect the geometry of the original grid. This assumption is correct if the fault is so narrow that it is not represented by a volumetric cell. The transmissibility between cell centers i and j now becomes,

$$T_{ij} = \frac{1}{T_i^{-1} + T_j^{-1} + T_f^{-1}} = \frac{1}{(T_{ij}^{TP})^{-1} + T_f^{-1}} = \frac{T_{ij}^{TP}}{1 + T_{ij}^{TP}/T_f} = m_{ij}T_{ij}^{TP}, \quad (15)$$

where we have used the definition of two-point transmissibilities and the well-know multiplier $m_{ij} = (1 + (T_{ij}^{\text{TP}}/T_f))^{-1}$. As pointed out in the introduction, one should note that the multiplier is a quantity that is grid specific and not associated with the fault itself. (The fault permeability K_f and the fault transmissibility density t_f , on the other hand, are not grid specific.) Now, we can use the relation

$$T_f = T^{\text{TP}} m_{ij} (1 - m_{ij})^{-1} \quad (16)$$

to calculate the fault transmissibility. If necessary, potential numerical artifacts of infinite or zero fault transmissibility when the fault multiplier is one or zero, respectively, can easily be removed by a careful implementation that uses static condensation or a combination of the formulations in Eq. 12 and Eq. 14.

Transmissibility multipliers are also used in real-field models to model shales that appear on a scale smaller than a single grid block. From a computational and physical point of view, such shales have a similar effect as a sealing fault in the sense that they represent barriers of small dimension with a transmissibility of relevance for the macroscopic flow. If information about the permeability and thickness of subgrid shales is available, we suggest to calculate the transmissibility in the same way as for sealing faults.

For models with sealing faults or subgrid shales, for which the multipliers are between zero and one, our overall method, presented in this and the previous section, gives a consistent and convergent discretization of a continuous problem defined by the tensor field \mathbf{K} on a domain Ω limited by outer boundaries $\partial\Omega$ and internal fault surfaces Γ with prescribed physical properties. However, some models can contain history-matched fault multipliers that are larger than unity. The physical interpretation of these is that the fault has caused fractures that increase the permeability in a direction perpendicular to the fault in the connecting cells. Such multipliers should be treated as a modification of the permeability of the cell in the given direction. For a mimetic method, one can alternatively modify the inner-product for the connecting cell, which would be equivalent to the normal method of handling multipliers for inner-products that become equivalent with the two-point method on a Cartesian grid.

Numerical Examples

In this section, we use four numerical examples to investigate the numerical properties of our method for representing and discretizing interior faults. The purpose of the first example is to compare the accuracy of three different discretizations for a 2D problem where we know the analytical solution: the two-point scheme (TPFA), the MPFA-O method (Aavatsmark et al., 2001) (which for $\eta = 0$ is identical to the TPFA method on a K-orthogonal grid), and a mimetic method (MFD) (Brezzi et al., 2005; Aarnes et al., 2008). The second example compares the performance of the three methods for a range of fault multipliers for a vertical fault, an inclined fault, and a curved fault. The third example is typical for many real-life model in which the combination of eroded layers and sloping faults makes it difficult to use standard stair-stepping techniques to avoid grid-orientation effects. Using a semi-synthetic model, we demonstrate how a consistent method can significantly improve the simulation accuracy. In the fourth and final example, we consider a simulation model of a reservoir offshore of Norway. Simulation results are provide both for the original model and for an areal grid derived by simplifying the full model.

Case 1: Vertical fault. We consider the rectangular domain $[-5, 5] \times [-4, 4]$ with a pressure drop from left to right and a single vertical fault at $x = 0, y \in [-2, 2]$ that is either fully open to flow or completely sealing. Both cases can obviously be handled by a standard discretization, leaving the grid unmodified in the open case and cutting cell connections over the fault in the sealing case. Here, however, we use the analytical solutions found for these two end-member cases to verify our general fault discretization. For the open fault, the analytical solution consists of a linear pressure drop from left to right. For the sealing fault, the pressure solution of a flow at an angle α to the fault is given in terms of a complex function

$$z = y - ix \quad p(x, y) = \Re(f(z)), \quad f(z) = z \cos(\alpha) - i\sqrt{z^2 - 4} \sin(\alpha).$$

The complex function is multivalued, and we use the following branch cut

$$\begin{aligned} \sqrt{z^2 - 4} &= \sqrt{r_1 r_2} \exp\left(\frac{1}{2}i(\theta_1 + \theta_2)\right), \\ z - 2 &= r_1 \exp(i\theta_1), \quad z + 2 = r_2 \exp(i\theta_2), \quad \theta_1, \theta_2 \in [0, 2\pi]; \end{aligned}$$

to pick the correct values, see, e.g., Churchill and Brown (1984) for more details. In both cases, we prescribe Dirichlet boundary conditions given by the analytical pressure solution.

We consider two grids, a regular Cartesian grid and a distorted grid transformed with

$$x = x + 0.1y \sin\left(\frac{2x\pi}{10}\right), \quad y = y + 0.9x \cos\left(\frac{y\pi}{8}\right) \left[1 - \left(\frac{2x}{10}\right)^2\right].$$

Figure 3 shows the results for linear flow with distorted grid and flow past the sealing fault for the Cartesian and the distorted grids. The two-point method is inconsistent on the distorted grid and hence exhibits a large error for the linear flow. The mimetic method is constructed to reproduce linear flow independent of the grid and hence has negligible error. For the sealing fault with Cartesian grid, the accuracy is approximately the same for all three methods. With a distorted grid, the main source of error for the two-point scheme comes from the grid-orientation effects (inconsistency), whereas the mimetic and the MPFA-O methods keep the error local around the fault also for distorted grid, as any consistent method should.

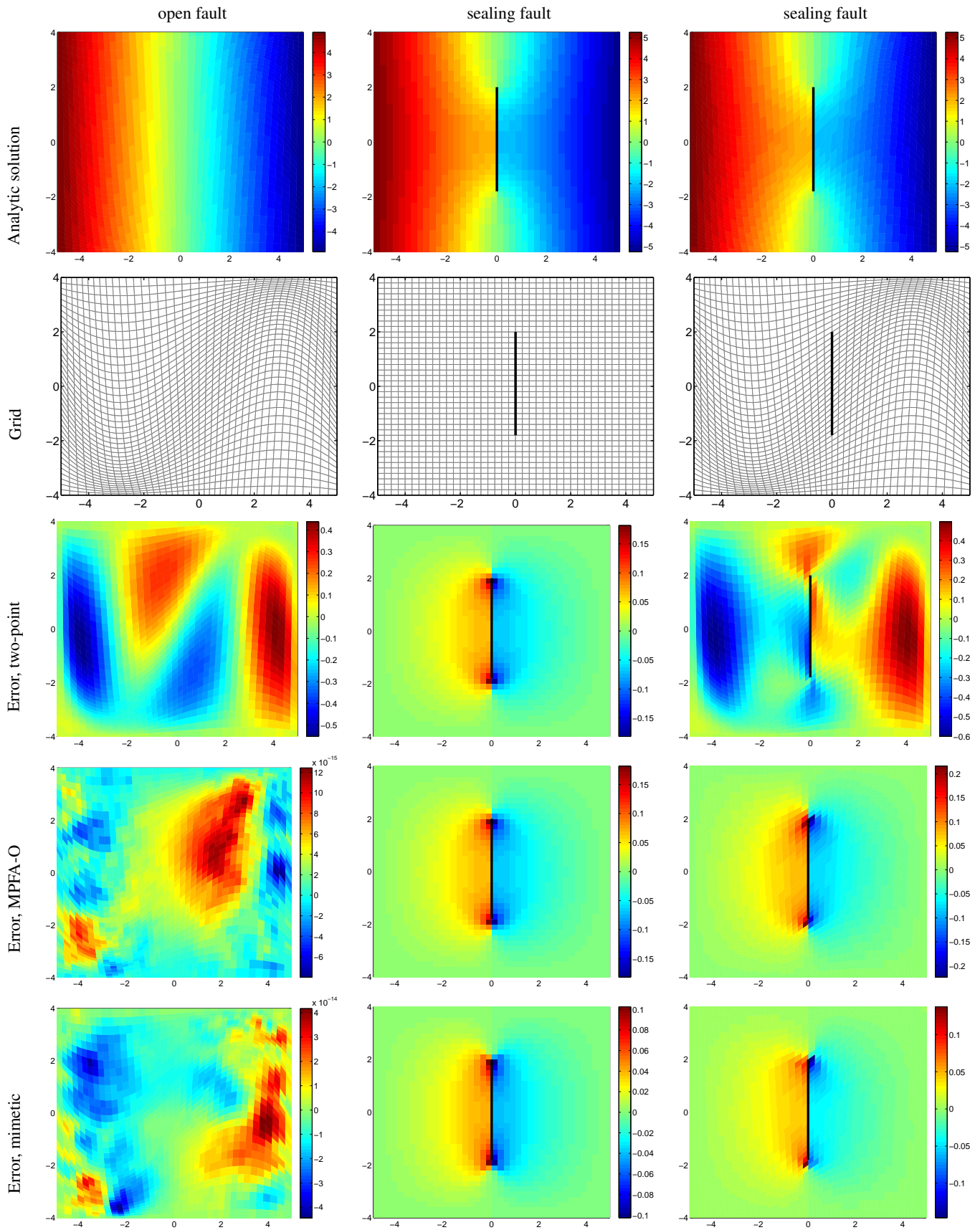


Fig. 3—Numerical study of a fully open and a sealing fault. The first row shows the analytical pressure solutions (in dimensionless units), the second row shows the grids, and the next three rows the pointwise L^∞ discretization errors.

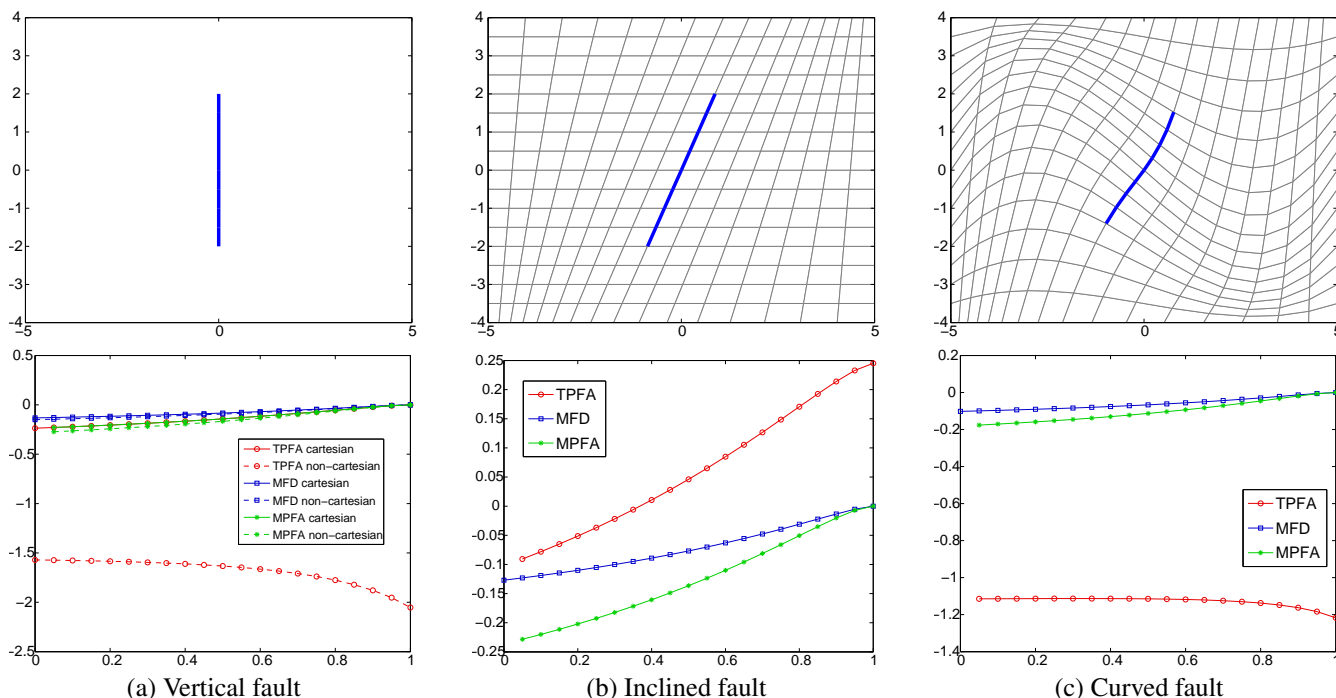


Fig. 4—Numerical study of varying fault multipliers for three different faults. The upper row shows the three different fault cases. The lower row shows the discrepancy in dimensionless flux compared with a reference solution as a function of multiplier value. The reference flux is obtained by refining two and four times and then doing a Richardson extrapolation.

Case 2: Varying multipliers. In the second test, we investigate the accuracy of the three schemes for a range of fault multipliers less than one. We consider three different types of faults: a vertical fault, an inclined fault, and a curved fault, see Figure 4. In all three cases, we prescribe pressures at the left and right boundaries with a pressure drop of ten, which would have given a unit Darcy velocity if the faults were not there. No-flow boundary conditions are prescribed along the top and bottom of the domain.

The flux over the right boundary is computed using different 16×16 grids. For the vertical fault, we use a Cartesian and a curvilinear grid as shown in the second row in Figure 3; for the inclined fault, we use a grid in which the angle of inclination of the grid lines in the y -direction varies from vertical to that of the fault and back again (upper-middle plot in Figure 4); and for the curved fault, we use a curvilinear grid in which the grid lines in the x -direction are almost perpendicular to the fault (upper-left plot in Figure 4). The plots in the lower row of Figure 4 show the discrepancies in flux compared with a fine-grid reference solution. The accuracy is comparable for all three schemes for the vertical fault with Cartesian grid, with mimetic being the most accurate. For the curvilinear grid, however, we see that the TPFA method gives completely wrong results, whereas the other two schemes retain their accuracy. For the second fault configuration, the distortion is less severe than in the previous case, and cancellations in errors because of symmetry give the somewhat surprising result that TPFA is more accurate than the other two schemes for multiplier values less than 0.65. On the other hand, the TPFA scheme fails to compute a correct flux for all multiplier values for the curved fault.

Figure 5 reports the result of a grid-refinement study on the three fault configurations. We see that whereas the mimetic scheme converges on all grids, the TPFA scheme only converges on the Cartesian grid for the vertical fault. The convergence for the MPFA-O scheme is similar as for the mimetic scheme and thus not reported.

The two examples above were chosen as simple as possible on purpose so that we could verify our method against analytical solutions. In practice, areal distortion of grids, as seen in the examples above, can easily be avoided using 2.5D Voronoi or fully unstructured grids. Likewise, highly deviated faults are commonly stair-stepped both areally and vertically to avoid grid distortions. However, it is not always possible to avoid introducing grid distortion. As an example of a particular challenge, we will in the following example consider the interaction of layer pinch-outs and sloping faults, which is commonly observed in real reservoirs. Here, it is very difficult to eliminate both types of grid distortions using unstructured or stair-stepped grids.

Case 3: Faulted model with lenses of low-permeable sand. In this example, we discuss grid deviations in the vertical direction introduced by the interaction of layer pinch-outs and sloping faults. To this end, we consider a set of semi-synthetic models obtained by introducing faults in a real-life model of a reservoir bed. The bed model consists of a good sand containing lenses of low-permeable sand, corresponding to a depositional environment in which flooding and erosion have been key processes. The erosion process will introduce a large number of pinched (vertically degenerate) cells. In addition, we have added a set of

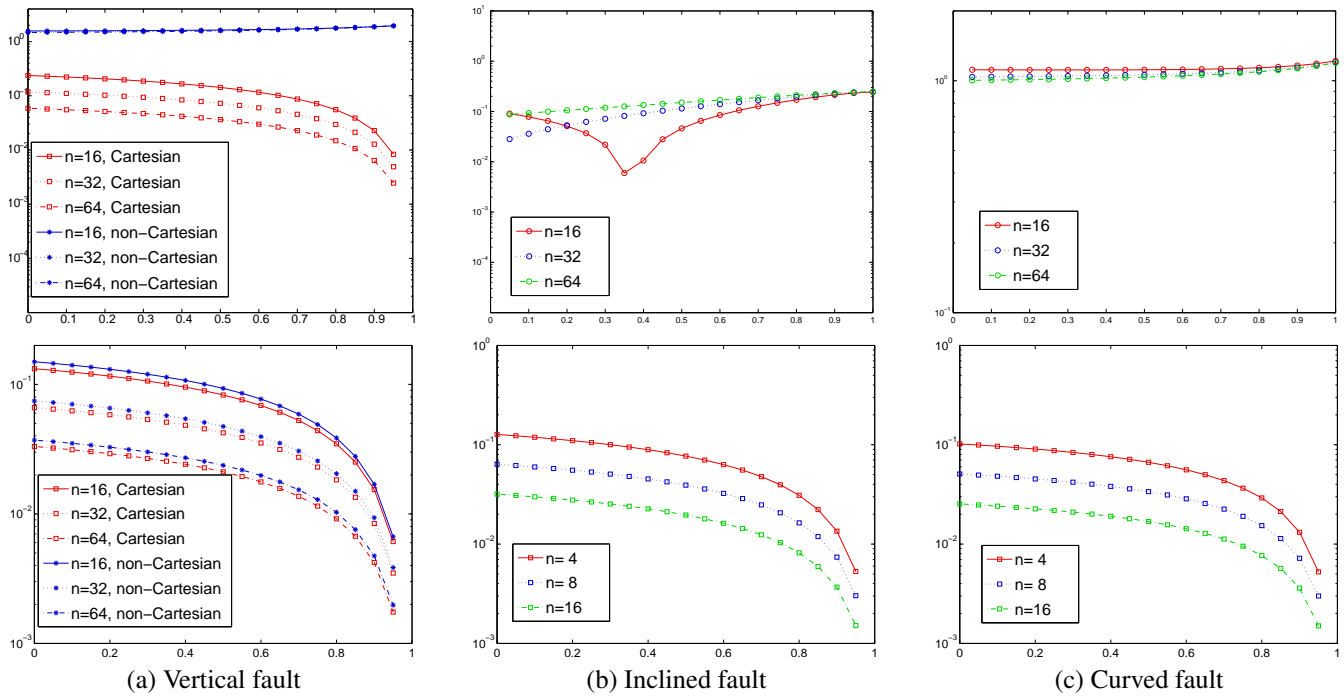


Fig. 5—Grid convergence study on a series of $n \times n$ grids for the three fault cases in Figure 4. The plots show the dimensionless flux error versus multiplier value for the TPFA scheme (upper row) and the mimetic scheme (lower row).

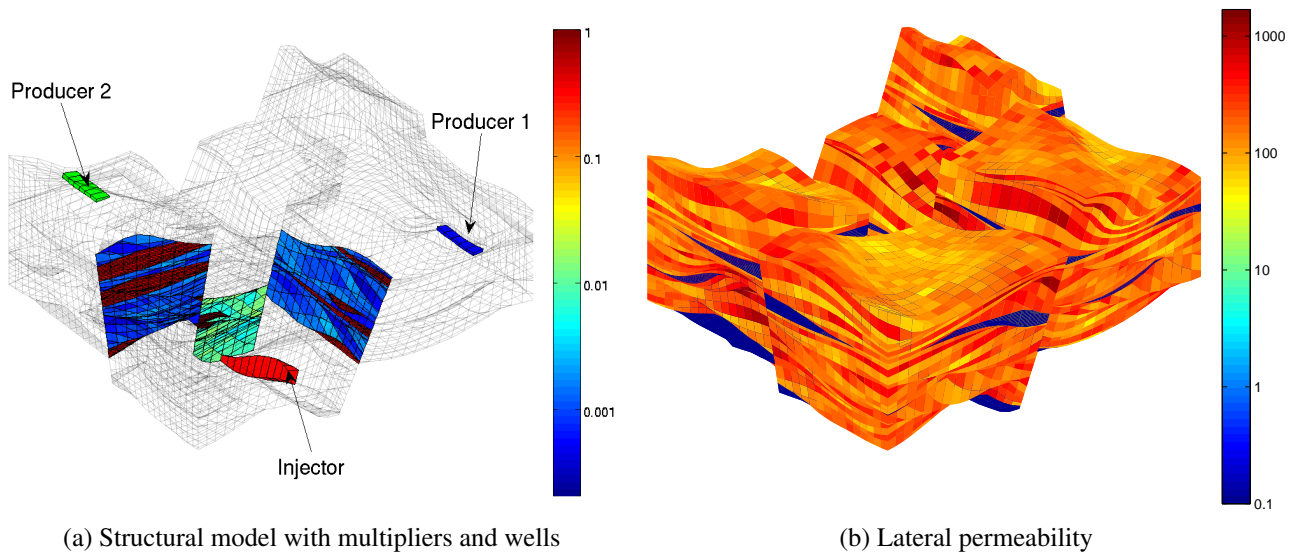


Fig. 6—The faulted model used in Case 3. (a) The plot shows the grid, the position of the cells containing the wells, and the three faults with reduced permeability (the color represents the logarithm of the corresponding multiplier values). (b) The plot shows the lateral permeability field (in milli Darcy on a logarithmic color scale). The vertical permeability is a factor ten smaller.

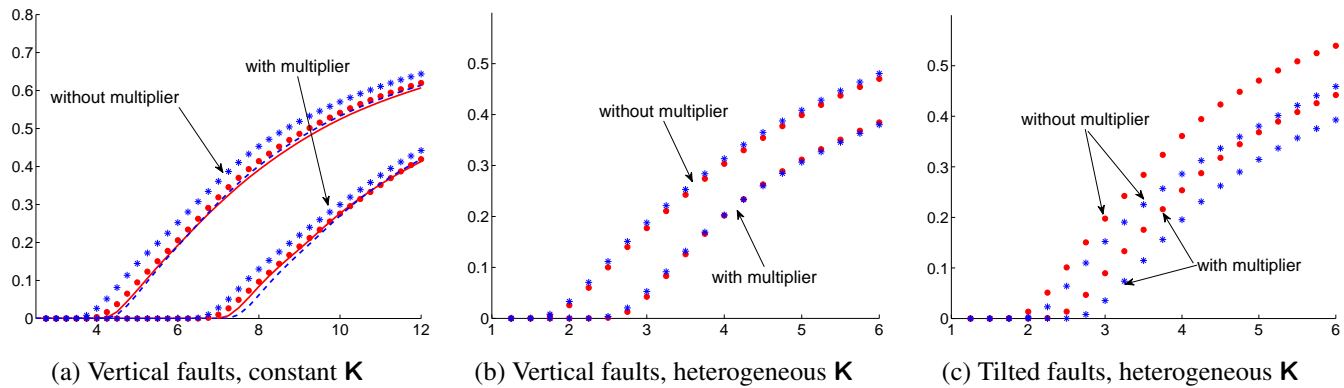


Fig. 7—The plots show the (dimensionless) water cut of producer number one (see Figure 6) as a function of time computed on the original grid with pinched cells, where the TPFA solution is shown as blue stars and the mimetic solution as red dots. In the left plot, the blue dashed and the red solid lines are the water cuts computed with the TPFA and the mimetic methods, respectively, on a grid with near uniform cells.

synthetic faults and introduced fault transmissibilities on some of the fault faces, see Figure 6. The fault transmissibilities are obtained from fault permeabilities varying between 10^{-2} and 10^{-3} milli Darcy and a fault thickness in the range of 0.1–1 meters. The reservoir is produced using three horizontal wells: one injector at the bottom and two producers along the top. The wells are set up so that both the faults and the heterogeneity caused by the low-permeable sand lenses will have an effect on the flow pattern.

Three factors will contribute to discrepancies between the TPFA and the mimetic method: (i) non-orthogonality and degeneracy (pinch-outs) in cells caused by the geological surfaces and sand lenses, (ii) heterogeneity in petrophysical parameters, and (iii) different treatment of fault multipliers. To isolate the effects, we start by introducing a set of *vertical faults* and disregarding the permeability variations by setting a homogeneous permeability in the whole structure. The left plot in Figure 7 shows a comparison of the TPFA and the mimetic solutions on two different grids: the original nonorthogonal grid with pinched cells used to model eroded layers and sand lenses and a more regular grid that only adapts to the top and bottom surfaces of the structure. For the regular grid, the discrepancies between the TPFA and the mimetic solutions (solid and dashed lines, respectively) are small. For the irregular grid from the original model there are distinct shifts in the TPFA solutions caused by grid-orientation effects, whereas the mimetic solutions remain almost the same, as should be expected since the two grids represent the same physical system (except for minor changes in the cell-wise representation of the wells).

In the middle plot of Figure 7, we have introduced the heterogeneous permeability, which here tends to reduce the differences between TPFA and the mimetic method. However, this situation changes dramatically when introducing the sloping faults, which together with the eroded layers force the grid cells to be far from orthogonal. As shown in the right plot in Figure 7, the discrepancy between the TPFA and the mimetic solutions are now much larger than acceptable; even larger discrepancies were observed for a homogeneous permeability. The example shows that tilted faults, pinched cells, and heterogeneity of the permeability all had effects on the water-cut curve. The combined effect is to introduce significant errors in the TPFA method and should, at least before a thorough investigation of grid-orientation effects has been conducted, discourage the straightforward application of this method. Mimetic or multipoint methods will provide a much more reliable alternative, when equipped with the ability to incorporate the sealing properties of the faults.

Case 4: Real-field model. In the last example, we consider the simulation model of a Norwegian offshore reservoir. The model consists of a $46 \times 112 \times 22$ logically Cartesian corner-point grid with 44,915 active cells. The geometry contains pinch-outs and eroded layers, giving four orders of magnitude differences in cell volumes and nine orders difference in face areas (for a single cell). The permeability spans four orders of magnitude in the lateral direction and five orders in the vertical direction and has lateral to vertical anisotropy ratios between 1.0 and 250. Altogether, there are 51 identified faults (with mismatched cells), out of which 32 are part of areally stair-stepped descriptions of deviated faults. In addition, there are thin shales represented as vertical transmissibility multipliers (associated with matching lateral faces). The well configuration consists of six injectors and thirteen producers.

For reference, we first illustrate the errors arising from not using a consistent discretization. To this end, we consider a single layer of the model and modify the geometry so that the thickness of the layer is constant and all pillars in the corner-point description are vertical. Wells are assigned by keeping one perforation for some of the original wells. For the TPFA and MPFA-O methods, we use the standard Peacemans well index, whereas for the mimetic method, we use numerically calculated well indexes (Ligardien, 2008). Moreover, we use a homogeneous permeability and set boundary conditions according to the

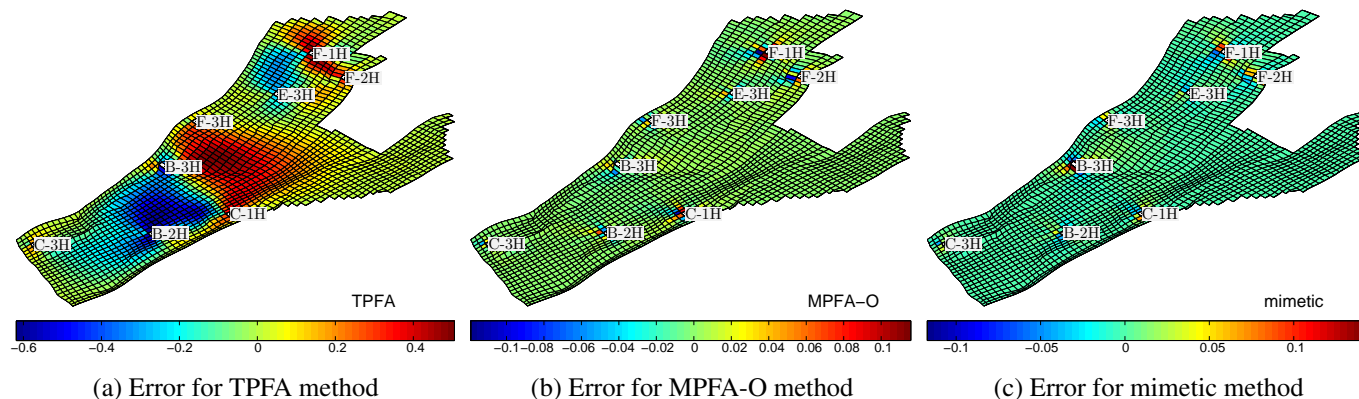


Fig. 8—Errors for the TPFA, MPFA-O, and the mimetic method (measured in dimensionless units) on a modified 2D slice of a real reservoir with uniform permeability and no fault multipliers.

analytical solution obtained for the prescribed well pattern in an infinite reservoir,

$$p(x, y) = \sum_i \frac{q_i}{2\pi K/\mu} \ln\left(\sqrt{(x - x_i)^2 + (y - y_i)^2}\right).$$

Figure 8 shows that the errors are small and local in the mimetic and MPFA-O methods, while they are up to 10 % and distributed all over the computational domain for the two-point method. These errors will most likely be larger for the full 3D model, which has erosions, pinch-outs, and skewed pillars, giving cells that degenerate and deviate far from being K-orthogonal. If we had used a regular Cartesian grid, the TPFA errors would also have been local and could have been completely adjusted for by the well index as first noted by Peaceman (1983). We therefore expect that the local errors for MPFA-O and the mimetic method on the unstructured grid could have been corrected for by a proper calculation of well indexes for these methods (i.e., so that the error is reduced to that of a Laplace flow with no wells).

Next, we introduce the heterogeneous permeability and the fault multipliers from the original model, see Figure 9, and consider flow under closed boundary conditions. The effect of the multipliers can clearly be seen for the fault that starts between wells F-1H and F-2H and ends up around F-3H. The cellwise discrepancies between MPFA-O and the mimetic method are less than 2–3 % of the pressure drop, whereas the discrepancies between the TPFA method and the other two methods are up to 10 %.

Finally, for comparative purposes and to demonstrate feasibility of our method, we consider the full 3D model and include the effects of fault transmissibility multipliers ranging from $7.5 \cdot 10^{-4}$ to 0.5 on the faults internal to model. The plots in the upper row of Figure 10 show face pressures along the faults computed using the mimetic and the TPFA method. Overall, the two solutions are qualitatively similar except that the TPFA solution shows a tendency of layering which is absent in the mimetic solution. This is particularly evident for the two faults in the upper 'finger' of the model, where the TPFA fault pressures are also somewhat lower. Given the complexity of the model, it is hard to tell whether the difference is caused by grid-orientation effects, differences in well modeling, or by the fact that face pressures are derived quantities in the TPFA method and computed quantities in the mimetic method. The lower row of Figure 10 shows the face pressures if we also include vertical transmissibility multipliers that model sub-grid shale layers, which introduce distinct jumps in the vertical pressure profiles.

Conclusions

We have discussed accurate modeling of faults as lower-dimensional objects and presented a new method for transforming two-point transmissibility multipliers so that they can be used in hybridized multipoint, mixed, and mimetic methods. The resulting discretization schemes have been verified against analytical solutions for two simple cases and against the traditional two-point method on grids where this method is correct. For all cases, the extended multipoint and mimetic discretizations were more accurate than the two-point method and, being consistent, they exhibited significantly less grid-orientation errors. Such errors are important for faulted reservoirs where the geology is dictated by complex fault networks; geometrically realistic models will then typically contain a lot of strongly distorted grid cells. Using lower-dimensional objects, rather than multipliers, gives a more geology-driven way of representing faults, and combining this approach with extended multipoint and mimetic schemes that are readily applicable to general polyhedral grids and less sensitive to grid distortion facilitates new ways of generating grids that reduce the errors in the geological representation. The advantage of using a consistent discretization scheme, combined with our new method for handling transmissibility multipliers, is demonstrated for two examples of realistic geologies, including the combination of sloping faults and eroded layers on a semi-synthetic model (Case 3) and areally stair-stepped faults in a real simulation model (Case 4).

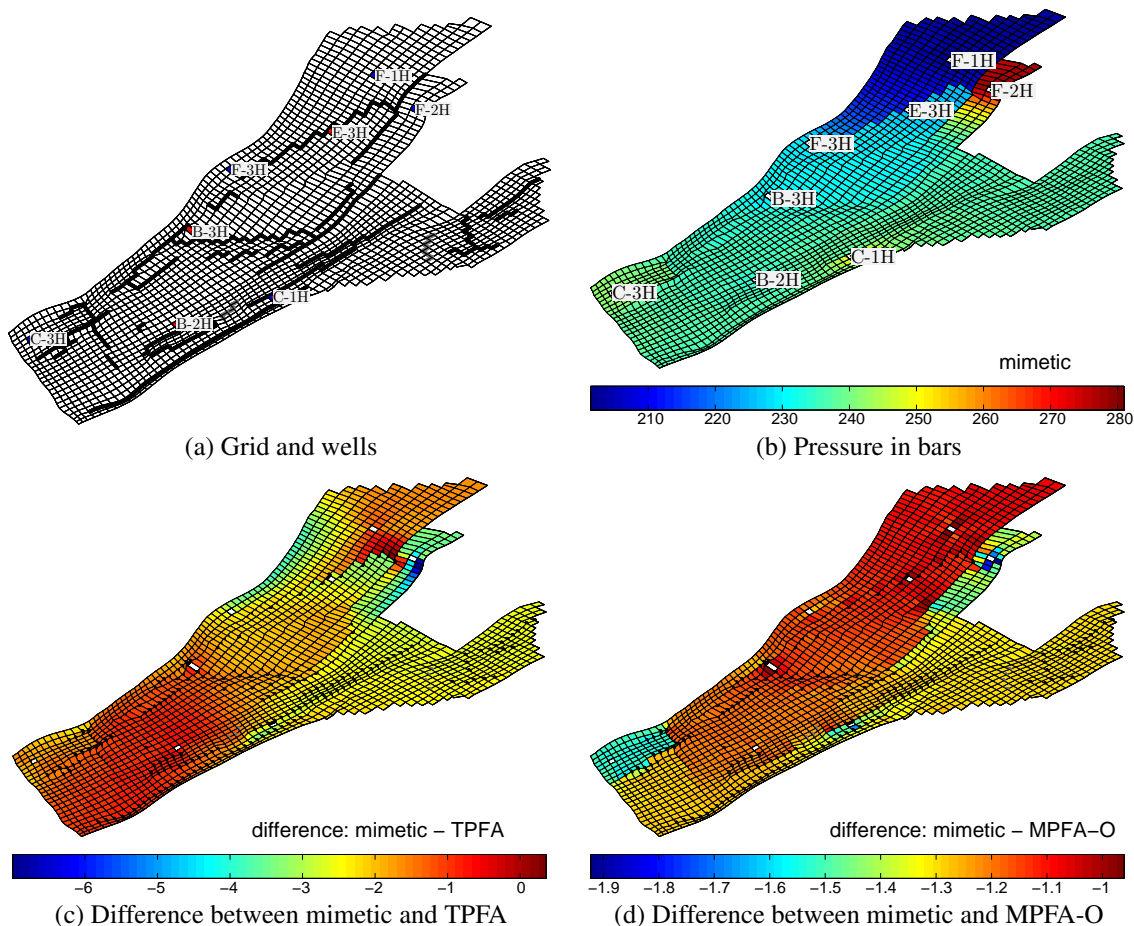


Fig. 9—(a) Wells and faults for a 2D slice of a real reservoir with heterogeneous permeability and fault multipliers. (b) The absolute pressure (in unit 'bars') calculated by the mimetic method. (c) The difference in pressure, measured in unit 'bars', between the TPGA and the mimetic method. (d) Pressure difference between the mimetic and the MPFA-O method.

Acknowledgments

The authors gratefully acknowledge financial support from the Research Council of Norway under grants number 175962 and 178013 and comments and suggestions from the three anonymous reviewers which helped to improve the paper.

Appendix: Error of using diagonal multiplier in the mimetic method

We consider one-dimensional flow in a homogeneous domain of length L that has a lower-dimensional fault in the middle. If v denotes the constant flux through any cross-section, and p_L and p_R the pressures at the end-points of the domain, we can express Darcy's law as follows:

$$v = mT(p_L - p_R), \quad (17)$$

where T is the transmissibility of the whole domain in the absence of a fault, and m is the domain-specific (but grid-independent) fault multiplier.

Next, we discretize the domain by two cells of equal size and let p_1 and p_2 denote the pressure at the cell centers and $\pi_{1/2} = p_L$, $\pi_{3/2}$, and $\pi_{5/2} = p_R$ the pressure at the cell interfaces. Using the one-sided transmissibilities from Eq. 4, we can write Darcy's law as

$$v = 2T^{\text{TP}}(\pi_{1/2} - p_1) = 2T^{\text{TP}}(p_1 - \pi_{3/2}), \quad (18)$$

where T^{TP} denotes the transmissibility between the pressures p_1 and p_2 at the cell centers. Assuming no fluid sources and using mass conservation in the first cell, we can write the two-point and the mimetic methods in hybrid form as follows,

$$\begin{bmatrix} a & b \\ b & a \end{bmatrix} \begin{bmatrix} -v \\ v \end{bmatrix} = \begin{bmatrix} p_1 - \pi_{1/2} \\ p_1 - \pi_{3/2} \end{bmatrix}, \quad (19)$$

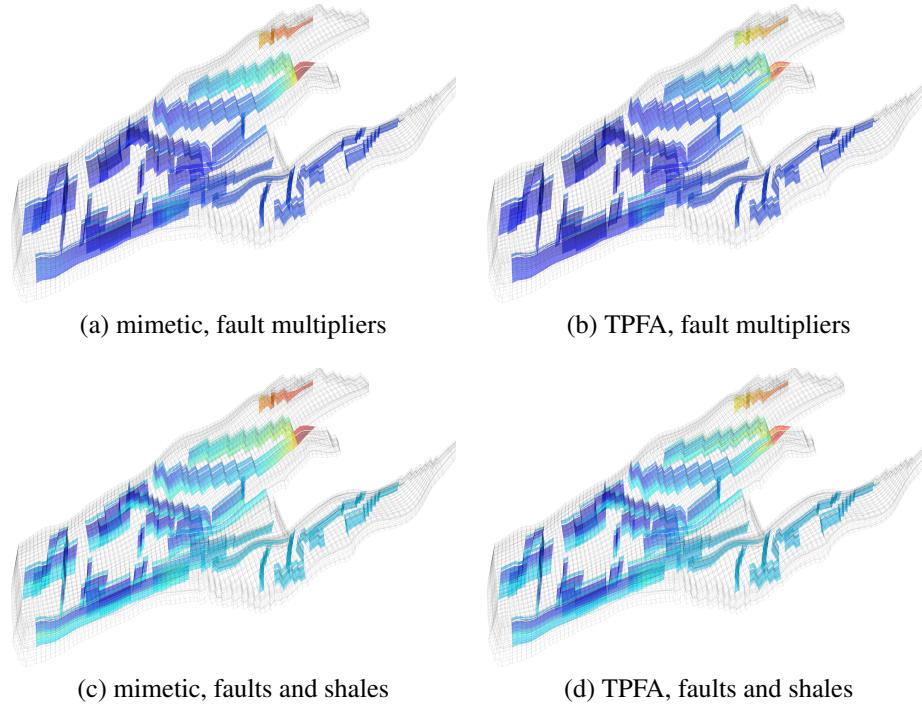


Fig. 10—Interface pressure values (in unit 'bars') along fault faces computed using the mimetic method and the TPFA method. Fault multipliers are included in (a) and (b); (c) and (d) also include multipliers modeling sub-grid shale layers.

where $a = 1/(2T^{\text{TP}})$ and $b = 0$ for the two-point method. To relate the mimetic method to the two-point method, we imposing Darcy's law from Eq. 18 to obtain that $a - b = 1/(2T^{\text{TP}})$. By making the choice that $a = a^{\text{TP}}/C$, the mimetic method then reads

$$\frac{1}{2T^{\text{TP}}} \begin{bmatrix} \frac{1}{C} & \frac{1}{C} - 1 \\ \frac{1}{C} - 1 & \frac{1}{C} \end{bmatrix} \begin{bmatrix} -v \\ v \end{bmatrix} = \begin{bmatrix} p_1 - \pi_{1/2} \\ p_1 - \pi_{3/2} \end{bmatrix}. \quad (20)$$

We now introduce a grid-dependent, two-point multiplier M at the interface in the middle of the domain. For the two-point method, this multiplier enters our discretization if we multiply element (2,2) of the matrix in Eq. 19 by $1/M$. The same simplified, but erroneous, approach is chosen for the mimetic method.

Using these two expressions, we will derive an analytic function for the error in v^{M} as a function of m . First, we find an expression for the pressure drop over the first cell by subtracting the first row in Eq. 19 from the second. For the two-point method, this gives

$$v^{\text{TP}} = \left[1 + \frac{1}{M} \right]^{-1} 2T^{\text{TP}} (\pi_{1/2} - \pi_{3/2}), \quad (21)$$

which coincides with the exact flux v , whereas for the mimetic method, we obtain

$$v^{\text{M}} = \left[\left(1 + \frac{1}{M} \right) \frac{1}{C} + 2 \left(1 - \frac{1}{C} \right) \right]^{-1} 2T^{\text{TP}} (\pi_{1/2} - \pi_{3/2}). \quad (22)$$

Using Eq. 21, the symmetry of the problem, and the fact that the medium is homogeneous, we can express the pressure drop over the whole domain as

$$v^{\text{TP}} = \left[1 + \frac{1}{M} \right]^{-1} T^{\text{TP}} (p_L - p_R). \quad (23)$$

In the absence of a fault, we see that $T = T^{\text{TP}}/2$, and by comparing Eq. 17 and Eq. 23, we see that the grid-dependent multiplier M is related to the domain-specific multiplier m through the expression $m/2 = (1 + M^{-1})^{-1}$. Inserting this expression into Eq. 21 and Eq. 22, and subtracting the latter from the former, we obtain an expression for the flux error as a function of m ,

$$\begin{aligned} E(m) &= v^{\text{M}} - v^{\text{TP}} = \left[\frac{1}{\frac{2}{m} \frac{1}{C} + 2 \left(1 - \frac{1}{C} \right)} - \frac{m}{2} \right] 2T^{\text{TP}} (\pi_{1/2} - \pi_{3/2}) \\ &= \frac{m(1-m) \left(1 - \frac{1}{C} \right)}{(1-m) \frac{1}{C} + m} T^{\text{TP}} (\pi_{1/2} - \pi_{3/2}). \end{aligned} \quad (24)$$

From this expression, we see that the error is zero in the special cases of $C = 1$ and $m = 0, 1$. The derivation can be extended verbatim to unidirectional flow in two and three spatial dimensions.

Nomenclature

Physical quantities:

p	=	pressure
π	=	face pressure
\mathbf{K}	=	absolute permeability r
t_f	=	fault transmissibility density
u_f	=	flux over face f
\vec{v}	=	total Darcy velocity
μ	=	fluid viscosity
q	=	volumetric rate

Domain and grid:

Γ	=	fault surface
Ω	=	entire physical domain
$\partial\Omega$	=	boundary of Ω
A	=	area of face
\vec{c}	=	vector: cell to face center
\vec{n}	=	normal vector to face

Vectors and matrices:

\mathbf{A}	=	matrix of face areas
\mathbf{B}	=	inner product of velocity basis functions
\mathbf{C}	=	integral of the divergence of velocity b.f.
\mathbf{D}	=	map from local to global face numbering
\mathbf{E}	=	matrix with fault transmissibilities
\mathbf{e}	=	identity vector
\mathbf{F}	=	inverse fault transmissibilities
\mathbf{N}	=	matrix of outer normal vectors
\mathbf{Q}	=	orthogonal decomposition of \mathbf{C}
\mathbf{T}	=	one-sided transmissibilities

Sub- and superscripts:

i, f	=	cell/face number
\pm	=	one-sided face values
TP	=	two-point scheme

References

- Aarnes, J. E., Krogstad, S., and Lie, K.-A. 2008. Multiscale mixed/mimetic methods on corner-point grids. *Comput. Geosci.*, 12(3):297–315. Doi: 10.1007/s10596-007-9072-8.
- Aavatsmark, I. 2002. An introduction to multipoint flux approximations for quadrilateral grids. *Comput. Geosci.*, 6:405–432. Doi: 10.1023/A:1021291114475.
- Aavatsmark, I. 2007. Interpretation of a two-point flux stencil for skew parallelogram grids. *Comput. Geosci.*, 11(3):199–206.
- Aavatsmark, I., Barkve, T., Bøe, Ø., and Mannseth, T. 1994. Discretization on non-orthogonal, curvilinear grids for multi-phase flow. *Proc. of the 4th European Conf. on the Mathematics of Oil Recovery*.
- Aavatsmark, I., Reiso, E., and Teigland, R. 2001. Control-Volume Discretization Method for Quadrilateral Grids with Faults and Local Refinements. *Comput. Geosci.*, 5:1–23. Doi: 10.1023/A:1011601700328.
- Aziz, K. and Settari, A. 1979. *Petroleum Reservoir Simulation*. Elsevier Applied Science Publishers, London and New York.
- Branets, L. V., Ghai, S. S., Lyons, S. L., and Wu, X.-H. 2009. Challenges and technologies in reservoir modeling. *Comm. Comput. Phys.*, 6(1):1–23.
- Brezzi, F. and Fortin, M. 1991. *Mixed and Hybrid Finite Element Methods*, volume 15 of *Springer Series in Computational Mathematics*. Springer-Verlag, New York.
- Brezzi, F., Lipnikov, K., and Simoncini, V. 2005. A Family of Mimetic Finite Difference Methods on Polygonal and Polyhedral Meshes. *Math. Models Methods Appl. Sci.*, 15:1533–1553. Doi: 10.1142/S0218202505000832.
- Churchill, R. V. and Brown, J. W. 1984. *Complex variables and applications*. McGraw-Hill Book Co., New York, fourth edition.
- Edwards, M. G. and Rogers, C. F. 1994. A flux continuous scheme for the full tensor pressure equation. *Proc. of the 4th European Conf. on the Mathematics of Oil Recovery*.
- Gringarten, E., Arpat, B., Haouesse, A., Dutranois, A., Deny, L., Jayr, S., Tertois, A., Mallet, J., Bernal, A., and Nghiem, L. 2008. New Grids for Robust Reservoir Modeling. In *SPE Annual Technical Conference and Exhibition, 21-24 September 2008, Denver, Colorado, USA*. SPE 116649-MS.
- Hoteit, H. and Firoozabadi, A. 2008. An efficient numerical model for incompressible two-phase flow in fractured media. *Adv. Water Resources*, 31:891–905.
- Klausen, R. A. and Stephansen, A. F. 2008. Mimetic MPFA. In *Proc. 11th European Conference on the Mathematics of Oil Recovery, 8-11 Sept., Bergen, Norway*, number A12. EAGE.
- Krogstad, S., Lie, K.-A., Nilsen, H. M., Natvig, J. R., Skaflestad, B., and Aarnes, J. E. 2009. A Multiscale Mixed Finite-Element Solver for Three-Phase Black-Oil Flow. Paper SPE 118993, presented at SPE Reservoir Simulation Symposium, The Woodlands, TX, USA, 2–4 February.
- Lie, K.-A., Krogstad, S., Ligaarden, I. S., Natvig, J. R., Nilsen, H. M., and Skaflestad, B. 2011. Open source MATLAB implementation of consistent discretisations on complex grids. Submitted. URL <http://www.sintef.no/project/MRST/mrst-comg.pdf>.

- Ligaarden, I. S. 2008. Well Models for Mimetic Finite Difference Methods and Improved Representation of Wells in Multiscale Methods. Master's thesis, University of Oslo. URL <http://www.duo.uio.no/sok/work.html?WORKID=77236>.
- Lipnikov, K., Shashkov, M., and Yotov, I. 2009. Local flux mimetic finite difference methods. *Numer. Math.*, 112(1):115–152. Doi: 10.1007/s00211-008-0203-5.
- Manzocchi, T., Walsh, J. J., Nell, P., and Yielding, G. 1999. Fault transmissibility multipliers for flow simulation models. *Petrol. Geosci.*, 5:53–63.
- Martin, V., Jaffré, J., and Roberts, J. 2005. Modelling fractures and barriers as interfaces for flow in porous media. *SIAM*, 26:1667–1691.
- MRST 2011. The MATLAB Reservoir Simulation Toolbox, Version 2011a. URL <http://www.sintef.no/MRST/>.
- Peaceman, D. 1983. Interpretation of Well-Block Pressures in Numerical Reservoir Simulation With Nonsquare Grid Blocks and Anisotropic Permeability. *SPE J.*, 23(3):531–543. Doi: 10.2118/10528-PA. SPE 10528-PA.
- Sperrevik, S., Gillespie, P. A., Fisher, Q. J., Halverson, T., and Knipe, R. J. 2002. Empirical estimation of fault rock properties. In Koestler, A. G. and Hunsdale, R., editors, *Hydrocarbon seal quantification: papers presented at the Norwegian Petroleum Society Conference, 16-18 October 2000, Stavanger, Norway*, volume 11 of *Norsk Petroleumsforening Special Publication*, pages 109–125. Elsevier.
- Wu, X.-H. and Parashkevov, R. R. 2009. Effect of grid deviation on flow solutions. *SPE J.*, 14(1):67–77. Doi: 10.2118/92868-PA.
- Yielding, G., Freeman, B., and Needham, D. T. 1997. Quantitative fault seal prediction. *AAPG Bull.*, 81(6):897–917.